Laser spectroscopy of the $3s\ ^2\Sigma^+ \leftarrow 2p\ ^2\Pi$ transition in LiNe

C. J. Lee and M. D. Havey
Department of Physics, Old Dominion University, Norfolk, Virginia 23529
(Received 10 December 1990)

Measurements of the rotationally resolved absorption spectrum of the $^6Li^{20}Ne$ and $^7Li^{20}Ne$ $3s\ ^2\Sigma^+ \leftarrow 2p\ ^2\Pi$ transition have been made. For each isotope, 13 vibrational transitions from the lower $2p\ ^2\Pi$ ($v''=0,1,2,3$) to the upper $3s\ ^2\Sigma^+$ ($v'=0,1,2,3,4,5$) electronic state have been observed and rotationally analyzed. For the $2p\ ^2\Pi$ state a well depth of 212(5) cm^{-1} and an equilibrium separation of $4.36(2)a_0$ have been obtained. Analysis of the $3s\ ^2\Sigma^+$ electronic state using an inverted perturbation analysis has revealed that the potential for this state displays, at large internuclear separations, a barrier greater than 60.6 cm^{-1} above the atomic Li $3s$ asymptote. The well region has a minimum of 570(7) cm^{-1} located at $4.11(1)a_0$. An anomalously large fine-structure constant of $A=2.77(3)$ cm^{-1} was determined for the $2p\ ^2\Pi$ ($v''=0$) level.

I. INTRODUCTION

Continuing spectroscopic studies[1–9] of alkali-metal–rare-gas diatomic molecules have recently provided accurate interaction potentials, in the normal range of chemical forces, for a number of states and of those molecules. The potentials find use in a wide range of collision studies of elastic and inelastic processes. Disagreement between spectroscopically determined excited-state potentials and calculated ones necessitate refinement of calculational techniques applied to weakly bound diatomic molecules.[10–25] Although significant convergence of experimental and theoretical results has been seen, in some cases there remains much room for improvement.

Rotationally resolved spectroscopy of the molecules and other approaches have also shown that, at short range, sizable magnetic interactions[1–5,7,8] may appear. For example, experiments have shown that for NaAr, NaKr, and NaXe, the spin-orbit coupling in the first excited $3p\ ^2\Pi$ state increases strongly with decreasing internuclear separation.[8,26] A similar but relatively much larger effect has been measured in the LiNe $2p\ ^2\Pi$ state; that result is described in this paper. In addition, gas-cell experiments on spin exchange between alkali metal and (odd-A) rare-gas ground-state atoms have shown the presence of a significant magnetic hyperfine interaction between the alkali-metal electron spin and the rare-gas nuclear spin.[27] Calculations have indicated that similar hyperfine interactions may exist in excited states of these molecules.[28] Λ doubling and spin-rotation couplings have also been measured in several experiments.[1–5,7–9]

We have an ongoing program of rotationally resolved spectroscopy of alkali-metal–rare-gas diatomic molecules; experimental results on the LiHe and LiHe $2p\ ^2\Pi$, $3s\ ^2\Sigma^+$, $3p\ ^2\Pi$, $3p\ ^2\Sigma^+$, $3d\ ^2\Pi$, $3d\ ^2\Sigma^+$, and $3d\ ^2\Delta$ states have been obtained.[6,9] Preliminary data on the LiAr $3s\ ^2\Sigma^+ \leftarrow 2p\ ^2\Pi$ spectrum have also been recorded. In the present paper we report details of experiments on the $3s\ ^2\Sigma^+ \leftarrow 2p\ ^2\Pi$ spectrum of LiNe. Analysis of the data has yielded accurate interaction potentials for those states and some information on the phenomena discussed in the previous paragraph. The following sections describe our experimental scheme and results. These then lead to analysis and discussion of the rotationally resolved spectra. Comparison is also made with other experimental and theoretical data on LiNe.

II. EXPERIMENT

The general experimental scheme is shown in Fig. 1, which illustrates qualitative interaction potentials for the first few molecular states of LiNe. In this scheme laser 1 resonantly excites Li atoms to the 2p state. Subsequent collisions with two Ne atoms produce bound LiNe molecules in the $2p\ ^2\Pi$ electronic state. Previous experiments[29,30] have shown that the relative atomic and molecular populations are nearly in thermal equilibrium at the gas temperature of about 350 K for a Ne pressure of 50 Torr. Laser 2 is scanned over the range of rovibrational transitions associated with the $3s\ ^2\Sigma^+ \leftarrow 2p\ ^2\Pi$ electronic transition. Molecular LiNe fluorescence on the bound-continuum $3s\ ^2\Sigma^+ \rightarrow 2s\ ^2\Sigma^+$ transition serves as the monitor of molecular LiNe absorption. The "collision-induced" excimer emission[31] occurs in a nearly featureless, approximately 13-nm-wide band centered at 395(3) nm. The analog of this emission band for LiAr, LiKr, and LiXe molecules has been previously reported by Wang and Havey.[32]

A schematic diagram of the experimental apparatus is presented in Fig. 2. The Li-Ne gas cell consists of a 250-cm^3 Pyrex flask mounted with 2.5-cm-diam entrance and exit ports and a 4.0-cm-diam fluorescence viewing port extending about 5 cm from the side of the flask. The laser-beam port windows are mounted at Brewsters angle. Metallic ^6Li or ^7Li is contained in an iron boat supported by a quartz tube; the top of the boat is located 1 cm below the center of the cell. A helically wound coaxial heater is located inside the boat and metallic Li is packed around the heater. Heating the boat at about 620 K produces an estimated Li density of about 10^{11} cm^{-3} in the

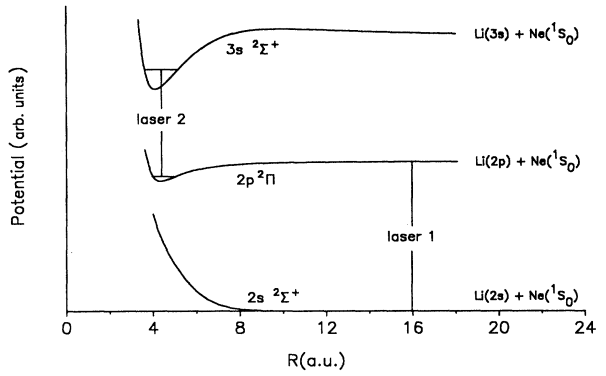

FIG. 1. Qualitative interaction potentials for several states of LiNe.

central region of the cell. The boat temperature is monitored by a single thermocouple mounted on the outside of the boat. The cell is attached to an oil-free vacuum-gas handling system; typical base pressure is about 10^{-7} Torr. Research grade neon of natural isotopic abundance is used with no further purification. The neon pressure is measured with an electronic capacitance manometer having a rated precision of better than 1%.

Both lasers 1 and 2 are Ar^+-laser pumped, standing-wave–cw dye lasers, and each produces a linearly polarized output of about 250 mW. Laser 1 is tuned to the atomic Li $2s$-$2p$ resonance transition at 671.0 nm by means of a birefringent filter–solid etalon combination. Its linewidth is about 0.20 cm^{-1}. Laser 2 is frequency scanned by a synchronously scanned three-plate birefringent filter–solid etalon combination. The details of the scanning method have been described in a previous paper.[9] With it, nearly linear scans of up to 30 cm^{-1} in length and a laser linewidth of 0.05 cm^{-1} are routinely achieved. Overlapping adjacent scans by 10.3 cm^{-1} allowed seamless reconstruction of the whole range of the measured spectrum.

The vacuum wave number of the laser 2 output was continuously monitored with a Fizeau wave meter having

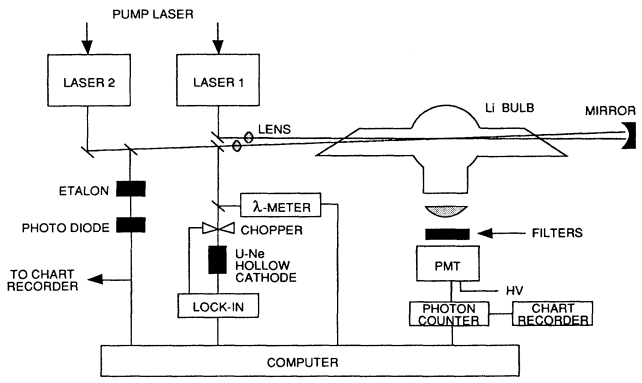

FIG. 2. A schematic diagram of the experimental apparatus.

an absolute accuracy of ± 0.005 cm^{-1}. The wave meter was calibrated in the 800–860-nm range by comparison with the absorption spectrum of a U-Ne hollow cathode lamp.[33] For the six calibration lines used, the absolute vacuum wave number as measured by the wave meter was in all cases within ± 0.02 cm^{-1} of tabulated values.

When laser 2 was tuned to a LiNe molecular absorption or to the atomic Li $2p$-$3s$ transitions at 812.8 nm, LiNe molecular emission in the bound-continuum $3s^2\Sigma^+ \rightarrow 2s^2\Sigma^+$ band at 395.0 nm was observed. This emission was virtually background free for Ne pressures below about 50 Torr and thus served as a monitor of molecular absorption. The blue molecular emission was collected and focused on the cathode of a bialkali-metal photomultiplier (PMT) tube. The tube was mounted with several colored glass filters that eliminated scattered laser light and the intense atomic Li 671.0-nm fluorescence. The glass filters had an effective bandpass of 30 nm centered at 400.0 nm. The PMT output was sampled at 10 Hz and processed by a photon-counting system.

A portion of the laser 2 output was chopped at 16 Hz and passed through the U-Ne hollow cathode. The hollow cathode signal was monitored with a lock-in amplifier tuned to the chopping phase and frequency. Another portion of the laser 2 output was passed through a 0.4987-cm^{-1} etalon and monitored by a photodiode. These two signals served as an absolute and relative frequency scale with which to calibrate and monitor the wave meter output.

Data acquisition and display were controlled by a laboratory computer. Four channels of data were recorded at a sampling rate of 10 Hz, synchronized with the wave-meter output. These included the wave-meter output, the photon-counter processed fluorescence signal, the lock-in output as driven by the hollow cathode, and the etalon signal as measured with the photodiode. The wave-meter output set the abscissa for the displayed spectrum while the photon-counter output determined the ordinate. The hollow cathode signal was also displayed, while the etalon signal was stored for later reference. Data were recorded and stored in 30-cm^{-1} segments; the acquired data were displayed in real time. While data files corresponding to adjacent scans could be merged into a continuous spectrum, we found it more convenient to make a chart recording of the molecular spectrum and etalon output. This recording was invaluable in initial rotational analysis of the spectrum. Final analysis and line position data were obtained from the computer data files. Absolute line positions were determined within ± 0.15 cm^{-1}.

III. RESULTS AND ANALYSIS

A. Overview of the spectrum

We have measured the LiNe $3s\,^2\Sigma^+ \leftarrow 2p\,^2\Pi$ absorption spectrum in the spectral range 11 680–12 400 cm^{-1}. In this range the dominant spectral feature is the collision-broadened atomic Li $2p$-$3s$ transitions[34] at 12 302.3 cm^{-1}; the 0.34-cm^{-1} splitting of this transition was clearly resolved. As mentioned previously, this tran-

sition and the molecular resonances were detected through the $3s\ ^2\Sigma^+ \rightarrow 2s\ ^2\Sigma^+$ excimer emission band at 395 nm. A scan over the spectral range 380–420 nm with a 0.3-m spectrometer having a resolution of about 2 nm revealed additional weak atomic Li emission lines. These lines corresponded to transitions[34] from the $5d$-$7d$ and $5s$-$8s$ Li levels to the $2p$ level. The appearance of the lines required that both lasers be tuned to atomic resonance. We attribute the lines to energy-pooling collisions in the Li vapor.

Upon scanning laser 2, 13 well-formed and intense rotation-vibration bands were observed. The peak intensity of the individual lines in the bands was 10^{-3}–10^{-4} of that of the atomic Li $2p$-$3s$ transition. A full width at half maximum of about 0.12 cm^{-1} was measured for the molecular signals; the width was very weakly dependent on Ne pressure in the 5–100-Torr range. No shift of the line positions with pressure was observed. The presence of the observed transitions required both Li($2p$) and Ne atoms in the cell; reducing the Ne pressure at nearly constant Li density resulted in a rapid decrease in the molecular signal.

Accompanying each band was a considerably weaker ($\sim$0.05 times the main band intensity), but nearly identical in form, rovibrational band. These bands were typically red-shifted about one wave number from the main band. The observed relative intensity is consistent with the natural abundances[35] of ^{20}Ne and ^{22}Ne. We have thus attributed the weaker transitions to be associated with the $^6Li^{22}Ne$ and $^7Li^{22}Ne$ $3s\ ^2\Sigma^+ \leftarrow 2p\ ^2\Pi$ electronic transition.

Each band consisted of three strong main $P(\Delta N=-1)$, $Q(\Delta N=0)$, and $R(\Delta N=+1)$ branches[36] and contained typically 30–60 individual transitions. The bands were largely blue degraded and showed a band head in the P branch. Several of the bands had nearly equal rotational constants in the lower and upper states, and their appearance and intensity was thus dominated by rotational distortion. They showed a second band head in the Q branch. Each band was also observed cut off abruptly with increasing rotation. As the cutoff occurred in each branch at the same amount N'' of lower $2p\ ^2\Pi(v'',N'')$ angular momentum, we attributed this to rotational predissociation[36] of the $2p\ ^2\Pi$ state.

For those bands originating in the $2p\ ^2\Pi(v''=0)$ level a well-resolved splitting of low N'' levels into fine-structure components with $J''=N''\pm\frac{1}{2}$ was also seen. The splitting decreased rapidly with increasing N'', as expected for a $2p\ ^2\Pi$ state undergoing a transition from Hunds case (a) to Hunds case (b) with increasing rotation.[36,37] No splitting due to a spin-rotation interaction was observed, nor were any combination defects[36] found in the measured combination differences. Various of the broad features of the spectrum discussed in this section may be seen in Fig.

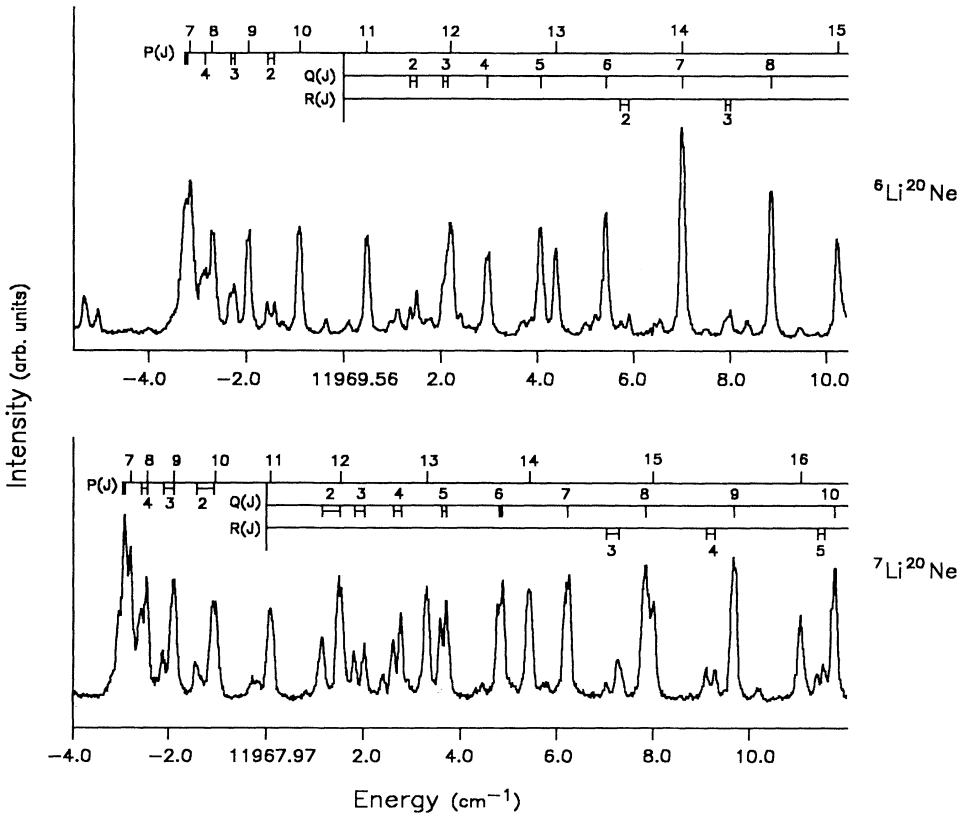

FIG. 3. The band origin region of the $3s\ ^2\Sigma^+(v'=0)\leftarrow 2p\ ^2\Pi(v''=0)$ transition in $^6Li^{20}Ne$ and $^7Li^{20}Ne$. Note the fine-structure splitting of the low-N lines.

3, which shows the $^6Li^{22}Ne$ and $^7Li^{22}Ne$ band origin region of the $3s\,^2\Sigma^+(v'=0) \leftarrow 2p\,^2\Pi_\Omega(v''=0)$ transition.

B. Spectral analysis

1. Rotation and vibration

For the $2p\,^2\Pi$ state a spin-orbit interaction nominally described by a spin-orbit parameter A_v is expected. Previous studies of this state in LiHe have shown that $A_v \lesssim 0.2\ cm^{-1}$, consistent with the view that the spin-orbit interaction is dominated by the interaction of the $2p$ electron with the Li^+ ion. However, significant splitting of low-N transitions out of $2p\,^2\Pi(v''=0)$ for LiNe indicate a much larger value of A_v for the $v''=0$ state. In this case the rotational energy levels, neglecting rotational distortion terms, are given by[36,37]

$$E_v(J) = B_v[(J+0.5)^2-1] \pm B_v(J+0.5)\left[1+\frac{Y(Y-4)}{4(J+0.5)^2}\right]^{1/2}. \quad (1)$$

In this equation J is the total angular momentum including spin and $Y = A_v/B_v$. This equation may be reexpressed in terms of the formal case (b) quantum number N by setting $J = N \mp 0.5$ and choosing the corresponding sign in (1). Then

$$F_1(N=J-\tfrac{1}{2}) = B_v[(N+1)^2-1] - B_v(N+1)\left[1+\frac{Y(Y-4)}{4(N+1)^2}\right]^{1/2},$$
$$F_2(N=J+\tfrac{1}{2}) = B_v(N^2-1)+B_vN\left[1+\frac{Y(Y-4)}{4N^2}\right]^{1/2}. \quad (2)$$

At large values of N, when the second term in the radical is small compared to 1, Eq. (2) reduces to the usual case (b) expression for a $^2\Pi$ state, $B_v[N(N+1)-1]$.

In spite of the fact that transitions from $N=21$ were the highest observed, it was necessary to include rotational distortion terms[36] of the form

$$-D_v[N(N+1)-1]^2+H_v[N(N+1)-1]^3 \quad (3)$$

in the fits to the data for the $2p\,^2\Pi$ state. No rotational distortion corrections to A_v were required. Furthermore, no splitting of higher N lines were observed and combination defects were unmeasurable within our experimental accuracy. Thus the combination of Eqs. (2) and (3) were sufficient to describe, within experimental precision, the measured rotational structure in the $2p\,^2\Pi_\Omega$ states. The rotational eigenenergies of the $3s\,^2\Sigma^+$ state were described by these two equations with $Y=0$ and $H_v=0$.

Measured term values for each band were then fit to the general form [36] $\nu = \nu_0(v',v'') + E(N') - E(N'')$, with $\nu_0(v',v'')$ the band origin and $E(N)$ the rotational energy for the upper and lower state. Assignments of the quantum numbers N were made through the usual first and second combination differences. The typical quality of these fits is illustrated in Fig. 4 by the second combination differences Δ_2 for the $3s^2\Sigma^+(0) \leftarrow 2p^2\Pi(1)$ band of

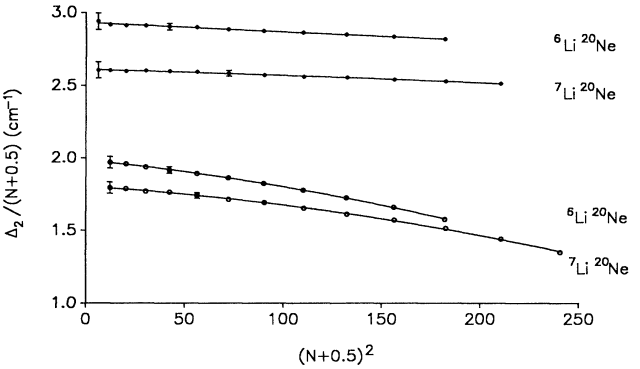

FIG. 4. Second combination differences for the $3s\,^2\Sigma^+(0) \leftarrow 2p\,^2\Pi(1)$ transitions of $^6Li^{20}Ne$ and $^7Li^{20}Ne$. Upper two curves, $3s\,^2\Sigma^+$; lower two curves, $2p\,^2\Pi$.

$^6Li^{20}Ne$ and $^7Li^{20}Ne$. The intercept of the fit is very nearly $4B_v$, while the slope for smaller N values is $8D_v$. The curvature in Δ_2 for the $2p\,^2\Pi(1)$ combination differences is due to $H_v \neq 0$. Values of B_v, D_v, and H_v thus obtained for the $2p^2\Pi$ and $3s^2\Sigma^+$ states are given in Table I.

As mentioned previously, a splitting of low-N transitions out of the $2p\,^2\Pi(v''=0)$ state was evident for both $^6Li^{20}Ne$ and $^7Li^{20}Ne$. No splitting was observed from transitions out of any $2p^2\Pi$ states with $v''>0$. The measured splittings were significantly greater for $^7Li^{20}Ne$. The line separations were fit to Eq. (2) and values of $Y=4.99(5)$ and $Y=4.48(5)$ were obtained for $^7Li^{20}Ne$ and $^6Li^{20}Ne$, respectively. Each of these values leads to a spin-orbit parameter $A=2.77(3)\ cm^{-1}$ for the $2p\,^2\Pi(v''=0)$ state. For $v''>0$, the absence of measurable broadening or splitting of low-N transitions within a limit of about $0.15\ cm^{-1}$ suggests [via Eq. (2)] that either $Y=4.3(3)$ or $Y \leq 0.3$ for those states. Further, due to the presence of weak $^{6,7}Li^{22}Ne$ transitions and line congestion in the band origin region, we are not able to unambiguously assign possible extra lines[36,38] corresponding to allowed case (a) ($\Delta J = \pm 1,0$) but forbidden case (b) ($\Delta N = \pm 2$) transitions. Thus, higher resolution data will be required to distinguish between the two possibilities.

For the $v''=0$ state, the value of $A=2.77(3)\ cm^{-1}$ is much larger than the value of $A=0.23\ cm^{-1}$ which would be expected [in a case (a) limit] if the valence electronic state was a $2p$ orbital centered on the Li^+ ion.[34] A possible explanation for this behavior of A is that the nominal Li $2p$ configuration becomes mixed with excitations of the Ne $2p^6$ configuration (for which the spin-orbit-interaction is quite large).[34] A similar, but fractionally much smaller effect has been measured[2,7,8,26] in the NaAr, NaKr, and NaXe $3p\,^2\Pi_\Omega$ states. It has been suggested (and disputed by Cooper[39]) that excitation of the Na $2p^6$ core is responsible for this. Although calculations are needed, perturbation of the $3p$ state by states associated with ground-state Na and excited-state rare-gas atoms is a likely explanation for the effect.

The band origins were determined by extrapolation of the Q branch to the rotationless state. After subtraction

TABLE I. Rotational constants for several $2p\ ^2\Pi$ and $3s\ ^2\Sigma^+$ vibrational levels of LiNe. All values are reported in vacuum cm^{-1}.

	$2p\ ^2\Pi$			$3s\ ^2\Sigma^+$	
v	B_v	$D_v\ (10^{-4})$	$H_v\ (10^{-6})$	B_v	$D_v\ (10^{-4})$
			$^6Li^{20}Ne$		
0	0.618(3)	0.53(15)	−0.30(3)	0.734(2)	0.80(10)
1	0.494(2)	1.31(23)	−0.52(6)	0.664(2)	0.84(6)
2	0.378(3)	3.27(32)		0.600(2)	0.80(7)
3	0.271(15)	4.39(1.58)		0.535(2)	0.93(7)
4				0.472(9)	0.64(1.09)
5				0.408(4)	1.42(27)
			$^7Li^{20}Ne$		
0	0.555(3)	0.51(12)	−0.19(2)	0.656(2)	0.63(8)
1	0.451(2)	1.16(22)	−0.31(6)	0.596(2)	0.66(6)
2	0.356(2)	2.95(8)		0.540(2)	0.66(6)
3	0.259(15)	3.27(1.58)		0.488(3)	0.71(9)
4				0.433(4)	0.72(18)
5				0.381(3)	0.97(13)

of the spin-orbit splitting, these are offset from $N=0$ by B_v''. Band origins, adjusted for the offset for all the observed transitions in $^6Li^{20}Ne$ and $^7Li^{20}Ne$, are given in Table II. These band origins, in combination with the rotational constants in Table I and the spin-orbit parameter $A=2.77(3)\ cm^{-1}$, reproduce nearly all the measured line positions to within about 0.15 cm^{-1}, within the uncertainty of the individual line positions. Tabulated values of the measured and fitted line positions are available from the authors.

The vibrational numbering in the $2p\ ^2\Pi$ and $3s\ ^3\Sigma^+$ states was determined from the measured isotope shifts[36] of the $^6Li^{20}Ne$ and $^7Li^{20}Ne$ band origins. Polynomial fits to the vibrational spacings then yielded the usual mechanical constants. These are presented in Table III. Also summarized in that table are the equilibrium rotational constants, obtained from least-squares fits to the vibration-dependent rotational constants given in Table I. Note that, particularly for the $2p\ ^2\Pi$ state, a large number of equilibrium constants are required to fit the data. This is a consequence of the exceptional anharmonicity of the $2p\ ^2\Pi$ state potential, which is also reflected in the large rotational distortion constants D_v and H_v. The ratio $\omega_e/\omega_e x_e$ of about 5 for this potential is quite small[40] compared to that for typical chemical bonds; a comparable value has been found for other weakly bound states such as the $B\ ^1\Pi$ state of LiH.[41]

2. *Analysis of results*

The data presented in the previous sections were further analyzed to obtain potentials for the $2p\ ^2\Pi$ and $3s\ ^2\Sigma^+$ electronic states. This was done through an inverted perturbation analysis[42] (IPA), the details of which have been presented elsewhere.[43] The basis functions used to generally describe the potentials were obtained from a variant of the Thakkar potential,[44] which is given as a power-series expansion in the quantity $\lambda=1-(R_e/R)^p$; R_e is the equilibrium internuclear separation and p a parameter. It was found convenient to express the potential for $R<R_e$ in a different manner than

TABLE II. Band origins for the various observed $3s\ ^2\Sigma^+(v')\leftarrow 2p\ ^2\Pi(v'')$ transitions in $^6Li^{20}Ne$ and $^7Li^{20}Ne$. The origins are expressed in vacuum cm^{-1}.

Isotope	v'',v'	$\nu_0\ (cm^{-1})$
$^6Li^{20}Ne$	0,0	11 969.6(2)
	0,1	12 106.0(2)
	0,2	12 222.7(1)
	1,0	11 895.8(1)
	1,1	12 032.3(2)
	1,2	12 149.1(2)
	1,3	12 248.6(1)
	1,4	12 331.4(1)
	2,0	11 851.9(2)
	2,3	12 204.6(3)
	2,4	12 287.4(2)
	2,5	12 354.0(2)
	3,0	11 826.5(1)
$^7Li^{20}Ne$	0,0	11 968.0(2)
	0,1	12 098.0(2)
	0,2	12 210.1(1)
	1,0	11 896.6(2)
	1,1	12 026.5(2)
	1,2	12 138.8(2)
	1,3	12 235.3(2)
	1,4	12 317.0(2)
	2,0	11 852.6(2)
	2,3	12 191.2(3)
	2,4	12 272.9(2)
	2,5	12 340.3(2)
	3,0	11 826.2(2)

TABLE III. Equilibrium vibrational and rotational mechanical constants for the $2p\,^2\Pi$ and $3s\,^2\Sigma^+$ states of $^6Li^{20}Ne$ and $^7Ni^{20}Ne$. All quantities are in cm^{-1}.

	$^6Li^{20}Ne$		$^7Li^{20}Ne$	
	$2p\,^2\Pi$	$3s\,^2\Sigma^+$	$2p\,^2\Pi$	$3s\,^2\Sigma^+$
B_e	0.684(5)	0.769(3)	0.609(5)	0.685(3)
α_e	0.133(8)	0.072(3)	0.110(8)	0.060(2)
γ_e	0.004(3)	0.0011(5)	0.0032(25)	0.0009(4)
ω_e	114.1(1.3)	158.9(1.7)	108.1(1.3)	150.0(1.4)
$\omega_e x_e$	23.2(6)	12.2(8)	21.0(6)	10.8(6)
$\omega_e y_e$	1.8(1)	0.68(22)	1.6(1)	0.53(17)
$\omega_e z_e$		0.04(2)		0.03(2)
D_0	161(5)		163(5)	

for $R > R_e$,

$$V(R) = \begin{cases} \sum_{i=0}^{1} \frac{e_i'}{R} \lambda^{2^{i+1}}, & R < R_e \\ \sum_{i=0}^{3} e_i \lambda^{2^{i+1}}, & R > R_e \end{cases} \quad (4)$$

Generally speaking, for $R < R_e$ the R^{-1} coefficient produces a hard repulsive wall, while the powers of λ having $p' < 0$, tend to soften it in an adjustable manner. For $R > R_e$, $p > 0$ and so $V(R)$ asymptotically approaches a constant dissociation energy Σe_i as $R \to \infty$. The two forms join smoothly at $R = R_e$.

Coefficients $[e_i, e_i', p(=-p')]$ describing the IPA $2p\,^2\Pi$ potential are given in Table IV. These coefficients describe a potential whose calculated eigenvalues for both isotopes agree with those generated from the data (Tables I and III) to less than ± 0.1 cm^{-1}. This potential, and the associated vibrational wavefunctions for $^6Li^{20}Ne$ for $v'' = 0, 1, 2, 3$, is shown in Fig. 5(a). The predicted well depth is $D_e = 211.9$ cm^{-1}.

As the observed rotational progressions in the data abruptly terminated with increasing N'' (due to rotational predissociation of the $2p\,^2\Pi$ state), the highest lying N'' levels from each vibrational state were initially omitted from the IPA data set. Subsequent inclusion of these levels did not lead to a significant increase in the IPA potential well depth, which is a quantity determined by the fit. Instead, the highest of the levels were predicted to be quasibound. This is consistent with the observed rapid decrease in the intensity of lines originating in these levels. For the $^6Li^{20}Ne$ $3s\,^2\Sigma^+(v'=5) \leftarrow 2p\,^2\Pi(v''=2)$ transition, a sharp decrease in intensity is measured for $P(12)$, $Q(12)$, and $R(12)$ compared to the $N''=11$ branch intensities. This behavior is seen in Fig. 6, which shows a portion of the band and the rotational assignment of the lines. The $N''=12$ level lies 220.1 cm^{-1} above the bottom of the $2p\,^2\Pi$ well and is clearly dissociated. On the other hand, the $N''=11$ level

TABLE IV. Parameters describing the IPA potentials for the LiNe $2p\,^2\Pi$ and $3s\,^2\Sigma^+$ states.

	$2p\,^2\Pi$		$3s\,^2\Sigma^+$	
	$R > R_e$	$R < R_e$	$R > R_e$	$R < R_e$
p	5.0		3.3	
e_0	189.2	684	749.54	3 196
e_1	7.5	7700	54.1	28 562
e_2	−11.9		84.4	
e_3	26.80		−282.9	
e_5 (*)			−34.40	
R_e (a.u.)	4.363		4.113	

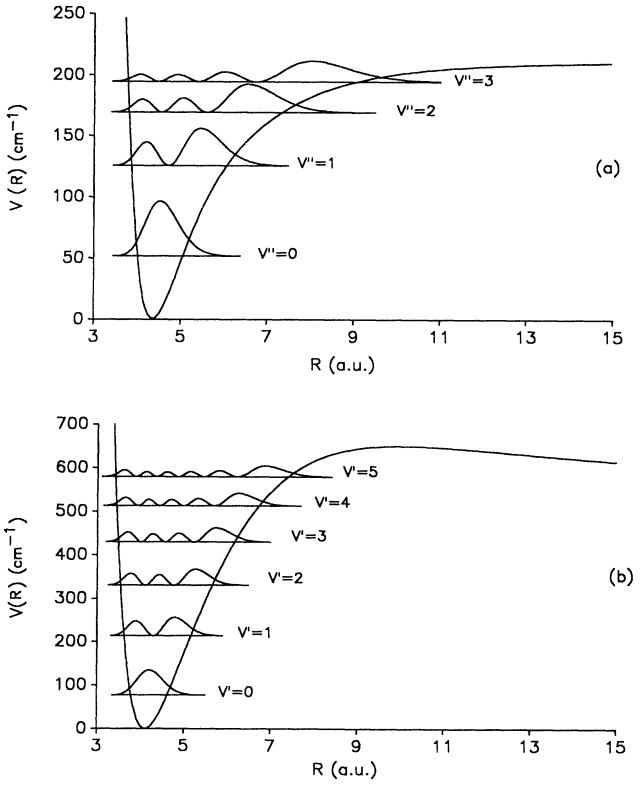

FIG. 5. IPA potentials and the vibrational wave functions for the LiNe $2p\,^2\Pi$ (a) and $3s\,^2\Sigma^+$ (b) states.

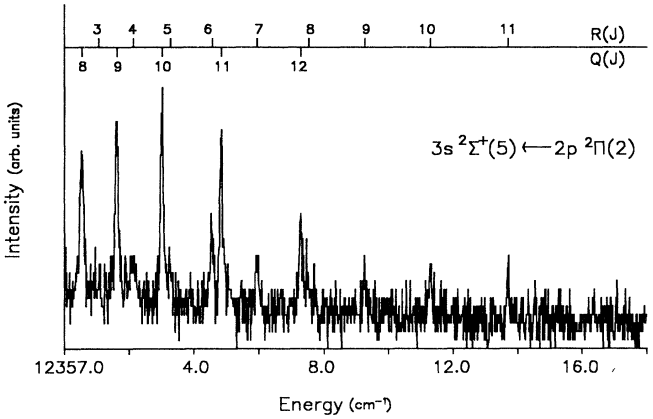

FIG. 6. A portion of the $^6Li^{20}Ne$ $3s\ ^2\Sigma^+(5)\leftarrow 2p\ ^2\Pi(2)$ rovibrational band, illustrating the effect of rotational predissociation in the $2p\ ^2\Pi(2)$ state.

at 213.2 cm^{-1} shows no evidence of predissociation in the data; the calculated IPA potential shows this level to be a quasibound state having most of its wave function inside the rotational barrier. Further, termination of the $v''=3$ P branch occurs above $N''=8$; the $N''=9$ level is at 215.2 cm^{-1} above the well minimum while $N''=8$ lies at 211.6 cm^{-1}. We conclude that the observed rotational predissociation in the $2p\ ^2\Pi$ state is entirely consistent with the IPA potential generated from the data, that potential having a depth of 212 cm^{-1} with an estimated uncertainty of about 5 cm^{-1}.

The set of coefficients describing the IPA potential for a $3s^2\ \Sigma^+$ state are presented in Table IV. The coefficients generate a potential whose eigenvalues for $^6Li^{20}Ne$ and $^7Li^{20}Ne$ agree with the experimental data to within ± 0.18 cm^{-1}. Of the 164 energy-level positions used in the fit, all but seven agreed with the IPA results within less than ± 0.10 cm^{-1}. As shown in Fig. 5(b), the potential has a maximum depth of 570.5 cm^{-1} relative to its $R\rightarrow\infty$ asymptote. However, a calculated barrier of 80.3 cm^{-1} peaked around $10.02a_0$ produces a well portion of 650.8 cm^{-1}. The energy levels used to produce the potential extend to 630.6 cm^{-1}, well above the asymptotic dissociation energy; many of these levels are then quasibound and unstable to decay via tunneling through the barrier. However, the barrier width is so large for these levels ($>7a_0$) that the vibrational wave functions have negligible amplitude in the outer region of the barrier.

The experimental data clearly show that there is a barrier in the $3s\ ^2\Sigma^+$ potential. A combination of the $2p\ ^2\Pi$ dissociation energy for each isotope with the 0-0 band origins and the atomic Li $2p$-$3s$ transition energy shows that the portion of the $3s\ ^2\Sigma^+$ potential below the Li ($3s$) asymptote has a depth of 570(7) cm^{-1}. The $v'=5$ vibrational level is at 581.6 cm^{-1}, and rotational levels extend to 630.6 and 60.6 cm^{-1} above the atomic dissociation asymptote. Thus a barrier of this height, or larger, exists in the $3s\ ^2\Sigma^+$ potential.

The IPA fitting procedure determines a potential only within the radial range for which discrete eigenenergies are available. For the $3s\ ^2\Sigma^+$ state this range extends from about $3.5a_0$ to $8.5a_0$. Outside this range only qualitative agreement at best can be expected with other results. The initial IPA fitting in fact predicted an asymptotic dissociation energy of 605.5 cm^{-1}, while the experimental value is 570(7) cm^{-1}. To produce the proper dissociation energy, we included an additional term in the expression for the potential. This term, indicated with an asterisk in Table IV, does not measurably change the calculated eigenvalues but does generate the proper asymptotic dissociation energy. Thus the shape of the IPA potential in the barrier region, outside the range of our data ($R\gtrsim 8.5a_0$) is not well determined experimentally. Additional data will be required to determine the full height of

TABLE V. Comparison of various determinations of the binding energy (D_e) and equilibrium separation (R_e) for the $2p\ ^2\Pi$ and $3s\ ^2\Sigma^+$ states of LiNe. The position and height of the barrier in the $3s\ ^2\Sigma^+$ potential is also given.

	D_e (cm^{-1})	$2p\ ^2\Pi$	R_e (units of a_0)
This experiment	212(5)		4.36(2)
Balling, Wright, and Havey *et al.* (Ref. 29)	225(30)		
Scheps *et al.* (Ref. 30)	<160		
Czuchaj and Sienkiewicz (Ref. 13)	22		7.5
Roberts (Ref. 25)	289.0		4.5
Pascale and Vandeplanque (Ref. 12)	16.9		8.0
Czuchaj *et al.* (Ref. 45)	166.0		4.0
	D_e (cm^{-1})	$3s\ ^2\Sigma^+$ Barrier (cm^{-1})	R_e (units of a_0)
This experiment	570(7)	>60.6	4.11(1)
Czuchaj and Sienkiewicz (Ref. 13)	71.3	454.7	5.25
Roberts (Ref. 25)	511.6	218.4	4.5
Pascale and Vandeplanque (Ref. 12)	134.4		5.75

the barrier and the quantitative shape of the long-range repulsive part of the $3s\ ^2\Sigma^+$ potential.

IV. DISCUSSION

For the $2p\ ^2\Pi$ state, the spectroscopic data reported in this paper extend in energy over the whole portion of the potential supporting bound states. We have thus been able to obtain a potential having an accuracy of about $\pm 5\ \text{cm}^{-1}$ in the dissociation energy, and about $\pm 0.1\ \text{cm}^{-1}$ over the range of the data. Higher resolution data would allow a better identification of the onset of rotational predissociation, and a refinement in the value of D_e.

Comparison of our results for the dissociation energy D_e and the equilibrium position R_e with others is made in Table V. Of these results, those from the line-broadening experiment of Balling, Wright and Havey[29] are in the best agreement with the dissociation energy reported here. The bound reported by Scheps *et al.*[30] is obtained from a $(0 \pm 5\ \%)$ limit on the measured pressure dependence of the $2p\ ^2\Pi \rightarrow 2s\ ^2\Sigma^+$ continuum emission spectrum in the range 40–600 Torr. Based on decreases in the continuum intensity with decreasing pressure for other molecules, the approximate limit in Table IV was obtained for LiNe and LiHe. However, our experiments[9,29] have shown that there is rapid teratomic molecular formation of LiHe and LiNe for as low a pressure as 50 Torr. If accurate lower pressure data could have been obtained in the difficult experiments of Scheps *et al.*,[30] it undoubtedly would have revealed the deeper LiHe and LiNe $2p\ ^2\Pi$ state potentials measured in this and other subsequent experiments.

Of the calculations on the LiNe $2p\ ^2\Pi$ state given in Table V, only the model potential results of Roberts[25] and the recent pseudopotential calculations of Czuchaj *et al.*[45] are in rough agreement with the experiment. In contrast with Roberts results for LiHe, where too shallow wells were predicted, the $2p\ ^2\Pi$ state well for LiNe is predicted to be about 25% deeper than that supported by experiment. The calculations of Czuchaj predict too shallow a $2p\ ^2\Pi$ well for LiNe. Some refinement of these calculations appears necessary. The results of Pascale and Vandeplanque[12] and the earlier results of Czuchaj and Sienkiewicz[13] show significantly weaker binding and well minima at large internuclear separations than the measurements. However, it is known that these calculations are most reliable for heavier rare-gas–alkali-metal binding where better agreement has been obtained in those cases.

A tabulation of experimental and theoretical results on the dissociation energy, barrier height, and equilibrium separation for the $3s\ ^2\Sigma^+$ state potential is made in Table V. The only experimental data of which we are aware are those presented in this paper. As discussed in Sec. III, the spectroscopic data determines the well region to within an accuracy of better than $\pm 0.2\ \text{cm}^{-1}$, and puts a lower bound on the height of the barrier. The peak wavelength (395 nm) of the $3s\ ^2\Sigma^+ \rightarrow 2s\ ^2\Sigma^+$ excimer emission band may be used to estimate the height of the repulsive $2s\ ^2\Sigma^+$ potential at the internuclear separation corresponding to the excimer emission peak. If we presume the main intensity to come from transitions out of the lower part[31] of the $3s\ ^2\Sigma^+$ potential, then the $2s\ ^2\Sigma^+$ potential should have a height of about $1300\ \text{cm}^{-1}$ at $R = 4.11 a_0$. These numbers are consistent with the results of Balling, Wright and Havey[29] if we set the radial scale of their potential by the $2p\ ^2\Pi$ state equilibrium radius $R = 4.36(2) a_0$ given in Table IV.

As was the case for the $2p\ ^2\Pi$ state, only the calculations of Roberts[25] are in reasonable accord with the experimental results, and significant discrepancies exist in that case as well. However, all of the calculations predict a barrier in the adiabatic potential at long range and a bound or quasibound region at smaller R, in qualitative agreement with experiment. A plausible origin of the repulsion barrier may be seen by inspection of the $3s$ radial wave function for atomic Li;[46] we presume that this is a good first approximation to the molecular electronic wave function. For this state there is a region of high electron density at larger e^--Li^+ separations corresponding to the outermost maximum in the electronic radial wave function. At smaller separations the electron density is proportionally much smaller. Thus as the Ne atom is brought from long range toward the Li atom, it initially encounters a repulsive electrostatic interaction with the Li atomic electron density. This effect may be modeled in terms of the asymptotic method introduced by Fermi,[47] where the interaction is thought of as the scattering of a free electron by the Ne atom; for s-wave scattering the repulsive interaction is then given in terms of the s-wave scattering length and the electron density at the Ne nucleus. The model potential calculations of Masnou-Seeuws[48] on excited states of KHe and KNe have shown this to be qualitatively correct, providing that the motion of the electron is taken into account. As the Li-Ne separation is made smaller, the electrostatic repulsion decreases, and is overcome by the attractive polarization interaction between the two atoms. If this explanation of the barrier in the $3s\ ^2\Sigma^+$ potential is correct, such barriers should be a common feature of the adiabatic potentials for these molecules. The calculations using the model potential of Peach[25] do show a long-range barrier in many of the adiabatic potentials.

V. CONCLUSIONS

In summary, we have reported detailed results on the rotationally resolved $3s\ ^2\Sigma^+ \leftarrow 2p\ ^2\Pi$ absorption spectrum of $^6Li^{20}Ne$ and $^7Li^{20}Ne$. The results have been analyzed to yield adiabatic potentials and dissociation energies for both states within the range of the data. For the $2p\ ^2\Pi$ state, the data extends over the full range of the potential, while for the $3s\ ^2\Sigma^+$ state it extends above the asymptotic dissociation energy. A barrier exists in the adiabatic potential for this state. For the $2p\ ^2\Pi$ state our results are in very good agreement with the line-broadening experiment of Balling, Wright, and Havey.[29] The model potential calculations of Roberts[25] are in good qualitative agreement with the experimental results for both states.

On a finer scale, an anomalously large spin-orbit coupling constant is measured for the $2p\ ^2\Pi(v''=0)$ level. The coupling is more than an order of magnitude larger than the asymptotic atomic Li value, indicating that states associated with the atomic Ne $2p$ shell must contribute to the nominal Li $2p$ configuration of the $^2\Pi$ state.

ACKNOWLEDGMENTS

We acknowledge useful discussions and the assistance of R. P. Meyer in the determination of the IPA potentials. The support of the National Science Foundation is greatly appreciated.

[1]R. Ahmad-Bitar, W. P. Lapatovich, D. E. Pritchard, and I. Renhorn, Phys. Rev. Lett. **39**, 1657 (1977).

[2]R. E. Smalley, D. J. Auerbauch, P. S. H. Fitch, D. H. Levy, and L. Wharton, J. Chem. Phys. **66**, 3778 (1977).

[3]J. Tellinghuisen, A. Rangone, M. S. Kim, D. J. Auerbauch, R. E. Smalley, L. Wharton, and D. H. Levy, J. Chem. Phys. **71**, 1283 (1979).

[4]W. P. Lapatovich, R. Ahmad-Bitar, P. E. Moskowitz, I. Renhorn, R. A. Gottscho, and D. E. Pritchard, J. Chem. Phys. **73**, 5419 (1980).

[5]R. A. Gottscho, R. Amhad-Bitar, W. P. Lapatovich, I. Renhorn, and D. E. Pritchard, J. Chem. Phys. **75**, 2546 (1981).

[6]M. D. Havey, Phys. Rev. Lett. **48**, 1100 (1982).

[7]G. Aepfelbach, A. Nunnemann, and D. Zimmermann, Chem. Phys. Lett. **96**, 311 (1983).

[8]E. Zanger, V. Schmatloch, and D. Zimmermann, J. Chem. Phys. **88**, 5396 (1988).

[9]C. J. Lee, M. D. Havey, and R. P. Meyer, Phys. Rev. A **43**, 77 (1991).

[10]J. Pascale, Phys. Rev. A **28**, 632 (1983).

[11]M. Phillipe, F. Masnou-Seeuws, and P. J. Valiron, J. Phys. B **12**, L493 (1979).

[12]J. Pascale and J. Vandeplanque, J. Chem. Phys. **60**, 2278 (1974).

[13]E. Czuchaj and J. Sienkiewicz, Z. Naturfursch. Teil A **34**, 694 (1979).

[14]W. E. Baylis, J. Chem. Phys. **51**, 2665 (1969).

[15]F. Masnou-Seeuws, J. Phys. B **15**, 883 (1982).

[16]R. P. Saxon, R. E. Olson, and B. Liu, J. Chem. Phys. **67**, 2692 (1977).

[17]G. Peach, Commun. At. Mol. Phys. **11**, 101 (1982).

[18]F. Masnou-Seeuws, M. Philippe, and P. Valiron, Phys. Rev. Lett. **41**, 395 (1978).

[19]R. Düren and G. Moritz, J. Chem. Phys. **73**, 5155 (1980).

[20]E. de Prunelé, Phys. Rev. A **35**, 496 (1987).

[21]M. Jungen and V. Staemmler, J. Phys. B **21**, 463 (1988).

[22]B. C. Laskowski, S. R. Langhoff, and J. R. Stallcop, J. Chem. Phys. **75**, 815 (1981).

[23]M. Dolan and F. Masnou-Seeuws, J. Phys. B **14**, L583 (1981).

[24]M. Krauss, P. Maldonado, and A. C. Wahl, J. Chem. Phys. **54**, 4944 (1971).

[25]G. Roberts (private communication). Potentials are calculated using the model potential of G. Peach.

[26]D. Zimmermann (private communication).

[27]See, for example, X. Zeng, Z. Wu, T. Call, E. Moron, D. Schrieber, and W. Happer, Phys. Rev. A **31**, 260 (1985).

[28]M. D. Havey and L. L. Vahala, Phys. Lett. A **125**, 47 (1987).

[29]L. C. Balling, J. J. Wright, and M. D. Havey, Phys. Rev. A **26**, 1426 (1982).

[30]R. Scheps, Ch. Ottinger, G. York, and A. Gallagher, J. Chem. Phys. **63**, 2581 (1975).

[31]F. Rostas, Spectral Line Shapes, edited by B. Wende (de Gruyter, City, (1981).

[32]W. J. Wang and M. D. Havey, Phys. Rev. A **29**, 3184 (1984).

[33]B. A. Palmer, R. A. Keller, and R. Engleman, Jr., Los Alamos Scientific Laboratory Informal Report No. LA-8251-MS, 1980 (unpublished).

[34]C. E. Moore, *Atomic Energy Levels,* Natl. Bur. Stand. Ref. Data Serv., Natl. Bur. Stand. (U.S.) Circ. No. 35 (GPO, Washington, D.C., 1971).

[35]*CRC Handbook of Chemistry and Physics,* 62nd ed., edited by Robert C. Weast and Melvin J. Astle (Chemical Rubber, Boca Raton, 1982).

[36]G. Herzberg, *Spectra of Diatomic Molecules* (Academic, New York, 1986).

[37]Hélène Lefebvre-Brion and Robert W. Field, *Perturbations in the Spectra of Diatomic Molecules* (Academic, New York, 1986).

[38]R. S. Mulliken, Rev. Mod. Phys. **3**, 89 (1931).

[39]D. L. Cooper, J. Chem. Phys. **75**, 4157 (1981).

[40]K. P. Huber and G. Herzberg, *Constants of Diatomic Molecules* (Van Nostrand Reinhold, New York, 1979).

[41]C. R. Vidal and W. C. Stwalley, J. Chem. Phys. **77**, 883 (1982).

[42]W. M. Kosman and J. Hinze, J. Mol. Spectrosc. **56**, 93 (1975).

[43]R. P. Meyer, M. D. Havey, and C. J. Lee (unpublished).

[44]A. J. Thakkar, J. Chem. Phys. **62**, 1693 (1975).

[45]E. Czuchaj, J. Rebentrost, H. Stoll, and H. Preuss, Chem. Phys. **136**, 79 (1989).

[46]Gary Simons, J. Chem. Phys. **60**, 645 (1974).

[47]E. Fermi, Nouvo Cimento **11**, 157 (1934).

[48]F. Masnou-Seeuws, J. Phys. B **15**, 883 (1982).